RESEARCH ARTICLE
SPACE PHYSICS: MAGNETOSPHERIC PHYSICS

Earth and Planetary Physics
6: 329–338, 2022
doi: 10.26464/epp2022037

Effects of polarization-reversed electromagnetic ion cyclotron waves on the ring current dynamics

MingHui Zhu[1,2], YiQun Yu[1,2*], Xing Cao[3], BinBin Ni[3,4], XingBin Tian[1,2], JinBin Cao[1,2], and Vania K. Jordanova[5]

[1]School of Space and Environment, Beihang University, Beijing 100191, China;

[2]Key Laboratory of Space Environment Monitoring and Information Processing, Ministry of Industry and Information Technology, Beijing 100191, China;

[3]Department of Space Physics, School of Electronic Information, Wuhan University, Wuhan 430072, China;

[4]Chinese Academy of Sciences Center for Excellence in Comparative Planetology, Hefei 230026, China;

[5]Space Science and Application, Los Alamos National Laboratory, Los Alamos, 87545, New Mexico, USA

Key Points:

- Polarization-reversed electromagnetic ion cyclotron (EMIC) waves generally reduce diffusion coefficients by a factor of 5–10 at different energies compared with the pure L-mode.
- The change in the proton precipitating flux caused by the reversal of polarization is not substantial from a global perspective.
- The ring current pressure is increased by approximately 10% at most with the inclusion of polarization reversal, suggesting a negligible impact.

Citation: Zhu, M. H., Yu, Y. Q., Cao, X., Ni, B. B., Tian, X. B., Cao, J. B., and Jordanova, V. K. (2022). Effects of polarization-reversed electromagnetic ion cyclotron waves on the ring current dynamics. *Earth Planet. Phys.*, *6*(4), 329–338. http://doi.org/10.26464/epp2022037

Abstract: Electromagnetic ion cyclotron (EMIC) waves are widely believed to play an important role in influencing the radiation belt and ring current dynamics. Most studies have investigated the effects or characteristics of EMIC waves by assuming their left-handed polarization. However, recent studies have found that the reversal of polarization, which occurs at higher latitudes along the wave propagation path, can change the wave-induced pitch angle diffusion coefficients. Whether such a polarization reversal can influence the global ring current dynamics remains unknown. In this study, we investigate the ring current dynamics and proton precipitation loss in association with polarization-reversed EMIC waves by using the ring current–atmosphere interactions model (RAM). The results indicate that the polarization reversal of H-band EMIC waves can truly decrease the scattering rates of protons of 10 to 50 keV or >100 keV in comparison with the scenario in which the EMIC waves are considered purely left-handed polarized. Additionally, the global ring current intensity and proton precipitation may be slightly affected by the polarization reversal, especially during prestorm time and the recovery phase, but the effects are not large during the main phase. This is probably because the H-band EMIC waves contribute to the proton scattering loss primarily at $E < 10$ keV, an energy range that is not strongly affected by the polarization reversal.

Keywords: electromagnetic ion cyclotron waves; polarization reversal; ring current

1. Introduction

Studying the plasma waves and their interactions with various plasma populations in the inner magnetosphere is crucial for understanding the dynamics of radiation belts and ring current. As one of the most important wave modes in the Earth's magnetosphere, electromagnetic ion cyclotron (EMIC) waves have frequently been observed in situ by satellites (Yuan ZG et al., 2010; Min et al., 2012; Allen et al., 2015, 2016; Saikin et al., 2015; Wang XY et al., 2017; Jun CW et al., 2019; Yue C et al., 2019; Blum et al., 2020) and ground-based stations (Perraut et al., 1984; Hendry et al., 2016; Engebretson et al., 2018a; Kim et al., 2020; Kwon et al., 2020). They are usually in the frequency range of 0.1–5 Hz and have three bands, which are separated by ion (H^+, He^+, O^+) gyrofrequencies (Young et al., 1981; Kozyra et al., 1984; Perraut et al., 1984; Engebretson et al., 2018a). EMIC waves have been considered to play a vital role in the magnetospheric dynamics because they can heat thermal plasma (Thorne and Horne, 1997; Zhang JC et al., 2010; Kitamura et al., 2018; Ma QL et al., 2019; Xue ZX et al., 2021) and scatter ring current ions (Jordanova et al., 2001; Xiao FL et al., 2011, 2012; Shreedevi et al., 2021; Zhu MH et al., 2021a) and radiation belt electrons (Lyons and Thorne, 1972; Jordanova et al., 2008; Su ZP et al., 2013; He FM et al., 2016; Li LY et al., 2016; Engebretson et al., 2018b; Ma X et al., 2020).

The generation of EMIC waves demands both an anisotropic ($T_\perp > T_{//}$) distribution of energetic (~10 to 100 keV) ring current ions (mostly protons), which provide the free energy for the instability (Cornwall, 1965; Kennel and Petschek, 1966; Rauch and Roux,

Correspondence to: Y. Q. Yu, yiqunyu17@gmail.com
Received 15 APR 2022; Accepted 02 MAY 2022.
Accepted article online 06 JUN 2022.

1982; Anderson et al., 1996; Wang Q et al., 2016; Zhu MH et al., 2021b), and cold plasma (e.g., H^+, He^+, O^+), which is considered the catalyst for wave generation by lowering the instability threshold and changing the wave growth rate (Cornwall, 1972; Young et al., 1981; Kozyra et al., 1984; Jordanova et al., 1996; Zhang JC et al., 2010). EMIC waves are usually generated as left-handed polarized (L-mode) waves near the equatorial region, and they propagate along the magnetic field line (Mauk and McPherron, 1980; Rauch and Roux, 1982; Hu YG et al., 2010; Allen et al., 2015). Additionally, some studies have demonstrated the existence of linearly polarized waves in the near dawn region owing to the generation of waves with oblique wave vectors (Anderson et al., 1992, 1996; Hu YG et al., 2010; Min et al., 2012). As the EMIC waves propagate along field lines to higher latitudes, the wave normal angles become much larger and the waves become more oblique, leading to the result that the wave frequency equals the crossover frequency (Rauch and Roux, 1982; Horne and Thorne, 1994; Anderson et al., 1996; Hu YG et al., 2010; Allen et al., 2015). At this point, it is possible for the waves to undergo a polarization reversal, transforming their polarization from left-handed to linearly or right-handed (Rauch and Roux, 1982).

Several researchers have studied the effects of the polarization-reversed EMIC waves. Cao X et al. (2020) found that including the polarization reversal of the H-band could increase the scattering rates of electrons > 4 MeV and decrease those of protons ranging from 10 to 50 keV or >100 keV, whereas the scattering rates associated with the He-band were almost unaffected. Lou YQ et al. (2021) performed parametric analyses of polarization-reversed EMIC waves and found that polarization reversal had remarkable effects on the diffusion coefficients for low pitch angles, indicating potential roles in the loss of ring current protons and radiation belt electrons. These studies imply that polarization reversal of EMIC waves may have nonnegligible effects on the ring current proton dynamics. However, in most previous studies that have modeled the scattering loss of ring current ions or radiation belt electrons, EMIC waves have been assumed to be purely left-handed for propagating strictly parallel to or obliquely to the magnetic field (Xiao FL et al., 2012; Usanova et al., 2014; Ni BB et al., 2015, 2018; Cao X et al., 2016, 2019; Capannolo et al., 2019; Shreedevi et al., 2021; Zhu MH et al., 2021a). Whether including the polarization reversal would affect the global ring current dynamics requires further study.

In the present study, we use the kinetic ring current–atmosphere interactions model (RAM) to investigate the potential effects of the polarization reversal on the ring current proton dynamics. The wave–particle diffusion processes in the model are determined by the bounce-averaged pitch angle diffusion coefficients obtained from either a purely left-handed EMIC wave or a more complicated EMIC wave with the high-latitude polarization reversal included. Comparisons between the two simulations revealed that the polarization-reversed H-band can indeed decrease the scattering rates of 10–50 and >100 keV protons and reduce the corresponding precipitation loss of energetic protons. However, from a global perspective, the effects on the ring current intensity and precipitating energy flux down to the upper atmosphere seem to be limited.

2. Model Description

To minimize the feedback effects of the electric and magnetic fields and better reflect the influence of only polarization reversal on the ring current dynamics, we use a dipolar version of Ring current–Atmosphere interaction model with Self-Consistent magnetic fields model, RAM-SCB (Jordanova et al., 2006, 2010; Zaharia et al., 2006, 2010), to simulate the effects of pitch angle diffusion in association with EMIC waves. The associated pitch angle diffusion coefficients are adopted from the full diffusion code (FDC; Ni BB et al., 2008, 2011; Shprits and Ni BB, 2009).

2.1 RAM Model

The RAM model is a kinetic ring current model (Jordanova et al., 2006, 2010). It solves the bounce-averaged Fokker–Planck equations, given as Equation (1) for ring current ions (i.e., proton, helium, and oxygen) and electrons (Jordanova et al., 2006, 2010):

$$\frac{\partial Q_l}{\partial t}+\frac{1}{R_o^2}\frac{\partial}{\partial R_o}\left(R_o^2\left\langle\frac{\mathrm{d}R_o}{\mathrm{d}t}\right\rangle Q_l\right)+\frac{\partial}{\partial\phi}\left(\left\langle\frac{\mathrm{d}\phi}{\mathrm{d}t}\right\rangle Q_l\right)+\frac{1}{\gamma p}\frac{\partial}{\partial E}\left(\gamma p\left\langle\frac{\mathrm{d}E}{\mathrm{d}t}\right\rangle Q_l\right)+\frac{1}{h\mu_o}\frac{\partial}{\partial\mu_o}\left(h\mu_o\left\langle\frac{\mathrm{d}\mu_o}{\mathrm{d}t}\right\rangle Q_l\right)=\left\langle\left(\frac{\partial Q_l}{\partial t}\right)_{loss}\right\rangle. \tag{1}$$

Here the angle brackets ⟨⟩ denote averaging during the bounce motion; the subscript l denotes the species and the subscript o denotes the magnetic equatorial plane; p is the relativistic momentum of the particle; γ is the Lorentz factor, which is calculated as $\gamma = 1 + E/\left(m_o c^2\right)$; $\mu_o = \cos\alpha_o$, where α_o is the equatorial pitch angle, which varies from 0° to 90°; R_o is the radial distance, which varies from 2 to $6.5R_E$, with $\Delta R_o = 0.25R_E$; and E is the kinetic energy, which varies from 0.15 to 400 keV. The loss processes in the model contain charge exchanges between neutral geocoronal hydrogen and ring current ions, atmospheric collisional loss, and pitch angle diffusion loss of electrons and ions. The EMIC wave scattering is considered the pitch angle scattering loss mechanism of the ions. The diffusion equations that solve the pitch angle scattering loss can be shown as follows:

$$\left\langle\left(\frac{\partial Q_l}{\partial t}\right)\right\rangle=\frac{1}{h\mu_o}\frac{\partial}{\partial\mu_o}\left[h\mu_o\left\langle D_{\mu_o\mu_o}\right\rangle\frac{\partial Q_l}{\partial\mu_o}\right], \tag{2}$$

$$\left\langle D_{\mu_o\mu_o}\right\rangle=\left(1-\mu_o^2\right)\left\langle D_{\alpha\alpha}\right\rangle, \tag{3}$$

where Q_l is the phase space distribution function; $\langle D_{\alpha\alpha}\rangle$ is the bounce-averaged pitch angle diffusion coefficient, obtained as described in Section 2.2. In the simulation, the dipolar magnetic field and *Kp*-based Volland–Stern empirical electric field (Volland, 1973; Stern, 1975) are used.

2.2 $D_{\alpha\alpha}$ Calculation Model

To calculate the bounce-averaged diffusion coefficients, the FDC is used. The wave spectral intensities of the three bands are assumed to be a Gaussian frequency distribution following previous studies (Glauert and Horne, 2005; Kersten et al., 2014):

$$I_B(\omega)=A\mathrm{e}^{-\left(\frac{\omega-\omega_m}{\delta\omega}\right)^2}\left(\omega_{lc}\leqslant\omega\leqslant\omega_{uc}\right), \tag{4}$$

where ω_{lc} and ω_{uc} are the lower and upper cutoff frequencies, respectively; ω_m is the peak wave frequency; $\delta\omega$ is the peak wave spectral bandwidth; and A is the normalization factor, which is a constant. The wave normal angle φ (the angle between the direc-

tion of propagation and the background magnetic field) is assumed to be a Gaussian distribution as follows:

$$g(\varphi) = e^{-\left(\frac{\tan\varphi - \tan\varphi_m}{\tan\varphi_\omega}\right)^2} \quad (\varphi_{lc} \leqslant \varphi \leqslant \varphi_{uc}), \tag{5}$$

where φ_{lc} and φ_{uc} are the lower and upper cutoff normal angles, respectively; φ_m is the wave angle with peak power, and φ_ω is the angular width. As we know, the polarization of electromagnetic waves is determined by the trajectory of the electric field vector with time. When the Doppler shift occurs, the cyclotron resonance relationship between an electromagnetic wave and a charged particle is as follows (Summers et al., 2007):

$$\omega - kv\cos\varphi\cos\alpha = \frac{N|\Omega_\sigma|}{\gamma}, \tag{6}$$

where ω is the wave frequency; k is the wave number; v is the speed of the particle; α is the pitch angle of the particle; N is the order of cyclotron resonance; Ω_σ is the gyrofrequency of the particle; and γ is the Lorentz factor: $\gamma = (1 - v^2/c^2)^{(-1/2)}$, where c is the speed of light. In the FDC, as waves travel from the equator toward higher latitudes, the wave normal angles ϕ increase gradually, which means the EMIC waves undergo a change from near the geomagnetic equator with parallel propagation to higher latitudes with much more oblique propagation. A detailed description of the latitudinally varying model of wave normal angle distribution can be seen in Ni BB et al. (2015). The polarization reversals occur at around crossover frequencies. Thus, the dispersive properties of EMIC waves are greatly altered by the polarization reversal, leading to changes in the diffusion coefficients. The two polarization approaches are described in detail in Cao X et al. (2020).

In the calculation, the nominal wave amplitude is set as 1 nT. The ion concentration ratio is adopted from previous studies (Summers et al., 2007; Cao X et al., 2020; Lou YQ et al., 2021) as $\eta_{H^+} : \eta_{He^+} : \eta_{O^+} = 0.85 : 0.1 : 0.05$, which is thought to be appropriate in numerical computation or theoretical analysis. The magnetic field is assumed to be dipolar. The electron number density, which is adopted from the plasmaspheric density model of Sheeley et al. (2001), is assumed to be constant along the magnetic field line. The contributions of cyclotron harmonic resonances from $N = -10$ to $N = 10$ are included. The typical wave spectrum of H-band EMIC waves, which follows previous studies (Albert, 2003; Summers and Thorne, 2003; Summers et al., 2007; Cao X et al., 2016, 2020; Lou YQ et al., 2021), is used: $\omega_{lc} = 0.5\Omega_{p,eq}$, $\omega_{uc} = 0.7\Omega_{p,eq}$, $\omega_m = 0.6\Omega_{p,eq}$, $\delta\omega = 0.1\Omega_{p,eq}$. The pitch angle diffusion coefficients are calculated in different f_{pe}/f_{ce} grids ranging from 2 to 20 with $\Delta f_{pe}/f_{ce} = 2$ and different L shells ranging from 3 to 7 with $\Delta L = 0.25$, where f_{pe} and f_{ce} denote the plasma frequency and electron gyrofrequency, respectively. The bounce-averaged $\langle D_{\alpha\alpha}\rangle$ as a function of f_{pe}/f_{ce}, E, α, L and magnetic local time (MLT), is determined from the FDC and is further scaled by the EMIC wave amplitude B_w as $D'_{\alpha\alpha} = \langle D_{\alpha\alpha}\rangle \times B_w^2$, which is then used in Equation (2) in the ring current model after interpolating $D'_{\alpha\alpha}$ into the model grids. The statistical wave intensity is based on Saikin (2018) and is auroral electrojet (*AE*) index dependent. The implementation of this statistical wave model has been described in Shreedevi et al. (2021) and Zhu MH et al. (2021a).

3. Simulation Results

In this study, the storm event on March 17, 2013, was simulated to investigate the effects of polarization reversal on ring current dynamics. Figure 1 presents the solar wind conditions and geomagnetic indexes (adopted from OMNIWeb, https://omniweb.gsfc.nasa.gov) during the storm, which began at approximately 6:00 universal time (UT) when the coronal mass ejection (CME) reached the Earth's magnetosphere, accompanied by the increases in solar wind speed, proton density, and dynamic pressure. The main phase of the storm lasted for approximately 14 hours, during which the disturbance storm time (*Dst*) index reached its minimum values at −100 nT and −132 nT at 10:30 UT and 20:00 UT, respectively. The pitch angle diffusion coefficients of the two polarization modes are adopted from the FDC as described above.

3.1 Distribution of $D_{\alpha\alpha}$

Figures 2a–2f show the equatorial global distributions of the bounce-averaged pitch angle diffusion coefficient $\langle D_{\alpha\alpha}\rangle$ calculated by using either pure left-handed (in Figures 2a and 2d) or polarization-reversed (in Figures 2b and 2e) H-band EMIC waves and their differences (in Figures 2c and 2f) at a pitch angle of α = ~5° during the main phase of the storm at 10:30 UT. The corresponding energies are 30, 164 keV, respectively. The difference D_m is calculated as follows: $D_m = \log_{10}(\langle D_{\alpha\alpha}\rangle|_{PR}/\langle D_{\alpha\alpha}\rangle|_{PL})$, where $\langle D_{\alpha\alpha}\rangle|_{PL}$ is the pitch angle diffusion coefficient from pure left-handed EMIC waves and $\langle D_{\alpha\alpha}\rangle|_{PR}$ is that with the inclusion of polarization-reversed EMIC waves. The D_m shows the difference in magnitude between the two quantities. In both cases, even with different energies, $\langle D_{\alpha\alpha}\rangle$ is maximized at similar locations: at 8 < MLT < 10 and L = 4–6, or at 17 < MLT < 21 and L = 5–6, extending to L < 4 at ~MLT = 21. The $\langle D_{\alpha\alpha}\rangle$ generally decreases with energy. Comparisons of $\langle D_{\alpha\alpha}\rangle$ in the two cases indicate that the $\langle D_{\alpha\alpha}\rangle$ with polarization reversal is slightly smaller than that of pure left-handed EMIC waves, which can be seen more clearly in their difference, represented by the D_m parameter in the last column of Figure 2. However, the discrepancies between the two cases appear to be energy dependent: at E = ~30 keV, the diffusion rates mainly decrease at L = 3–6 and MLT = 9–19; at E = ~164 keV, the difference D_m is evident mainly at L = 4–6 and MLT = 12–21. Figures 2g–2h show the bounce-averaged pitch angle diffusion coefficient $\langle D_{\alpha\alpha}\rangle$ of protons as a function of energy and pitch angle for H-band EMIC waves at MLT = 15 at L = 5.5. The difference in $\langle D_{\alpha\alpha}\rangle$ between pure left-handed polarization and polarization reversal is also shown in Figure 2i. The difference is about one order of magnitude at E = 15–60 keV for pitch angle $\alpha < 50^\circ$, and the difference can be larger than two orders of magnitude for E > 100 keV and $\alpha < 30^\circ$.

We find that the global distribution of the difference D_m is actually closely related to the local f_{pe}/f_{ce}. Figures 3a and 3b further show the difference D_m at E = ~4 keV and 12 keV, α = ~5° at 10:30 UT. Figure 3c shows the global distribution of f_{pe}/f_{ce}. The difference in $\langle D_{\alpha\alpha}\rangle$ at low energies (E approximately equal to a few kiloelectron volts to tens of kiloelectron volts) is notable inside the plasmapause where f_{pe}/f_{ce} is larger than 10, whereas the difference in $\langle D_{\alpha\alpha}\rangle$ for large energies (e.g., E > 100 keV in Figure 2f) is large outside the plasmapause, where f_{pe}/f_{ce} is smaller, as well as in the plume,

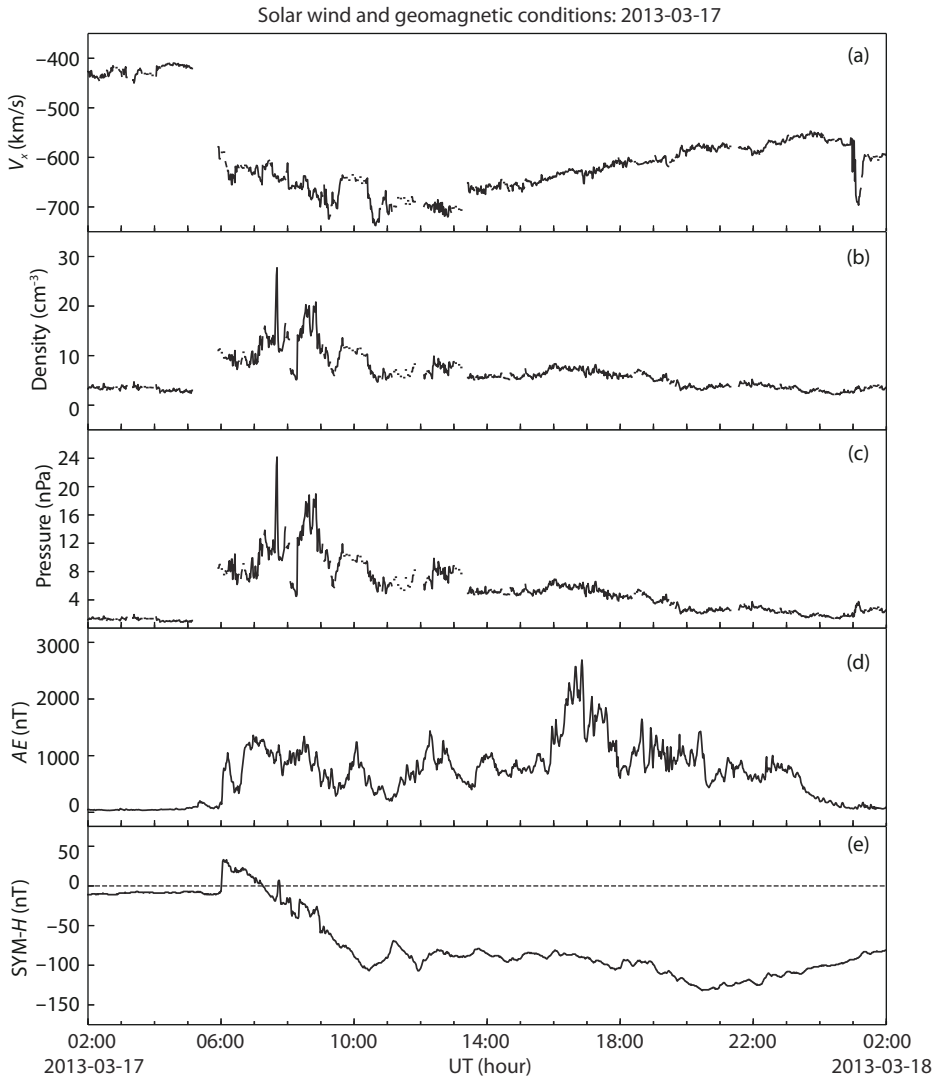

Figure 1. Interplanetary solar wind parameters for the interval from 02:00 universal time (UT) on March 17, 2013, to 02:00 UT on March 18, 2013, from OMNI (http://omniweb.gsfc.nasa.gov/). (a) V_x component of the solar wind speed, (b) proton density, (c) pressure, (d) auroral electrojet (*AE*) index, and (f) symmetric *H*-component (SYM-*H*) index.

where f_{pe}/f_{ce} is >14. Figures 3d–3f illustrate the $\langle D_{\alpha\alpha}\rangle$ as a function of pitch angle with different energies at three selected locations (denoted by the white dots in Figure 3c). With f_{pe}/f_{ce} = 10 inside the plasmasphere in the dusk sector (Figure 3d), the largest difference between the $\langle D_{\alpha\alpha}\rangle$ in the two polarization modes is at E = ~30 keV (comparing the purple lines). For f_{pe}/f_{ce} = 16 in the dayside plume (Figure 3e), the most significant change in $\langle D_{\alpha\alpha}\rangle$ in the two polarization modes is at E = ~12 keV and 164 keV. Outside the plasmasphere, as the f_{pe}/f_{ce} is close to 2, $\langle D_{\alpha\alpha}\rangle$ is influenced only at E = 164 keV when the polarization reversal is considered. Among all these different locations and energies, the largest change in the $\langle D_{\alpha\alpha}\rangle$ can be seen to lie in energies >100 keV inside the plume, whereas the change in other energies is no more than merely one order of magnitude.

3.2 Effects on the Precipitation Loss

To investigate the effects of these different pitch angle diffusion coefficients $\langle D_{\alpha\alpha}\rangle$ on ring current ions more directly, the $\langle D_{\alpha\alpha}\rangle$ at pitch angle α = ~5° and the precipitating flux of protons as a function of energy are shown in Figure 4. From left to right, three times are chosen: T = 3:00 UT, 10:30 UT, and 1:00 UT (on the next day), to represent the prestorm, main phase, and recovery phase of the storm. After the polarization reversal is included (dashed lines), the $\langle D_{\alpha\alpha}\rangle$ is slightly decreased at energies ranging from several kiloelectron volts to tens of kiloelectron volts and at energies >100 keV. Consistent with the $\langle D_{\alpha\alpha}\rangle$, the precipitating flux of protons during the prestorm and recovery phase (Figures 4d and 4f) also decreases at the energy ranges mentioned. However, the change in the precipitating flux at 10:30 UT (Figure 4e) is small enough to be negligible. The reason the polarization-reversed $\langle D_{\alpha\alpha}\rangle$ during the main phase of the storm has limited effects on the precipitating flux may be because more isotropic source plasma is injected into the ring current during the storm time and the diffusion is less effective on an isotropic distribution. Thus, even with a reduced $\langle D_{\alpha\alpha}\rangle$, the difference in the precipitating flux is not as large.

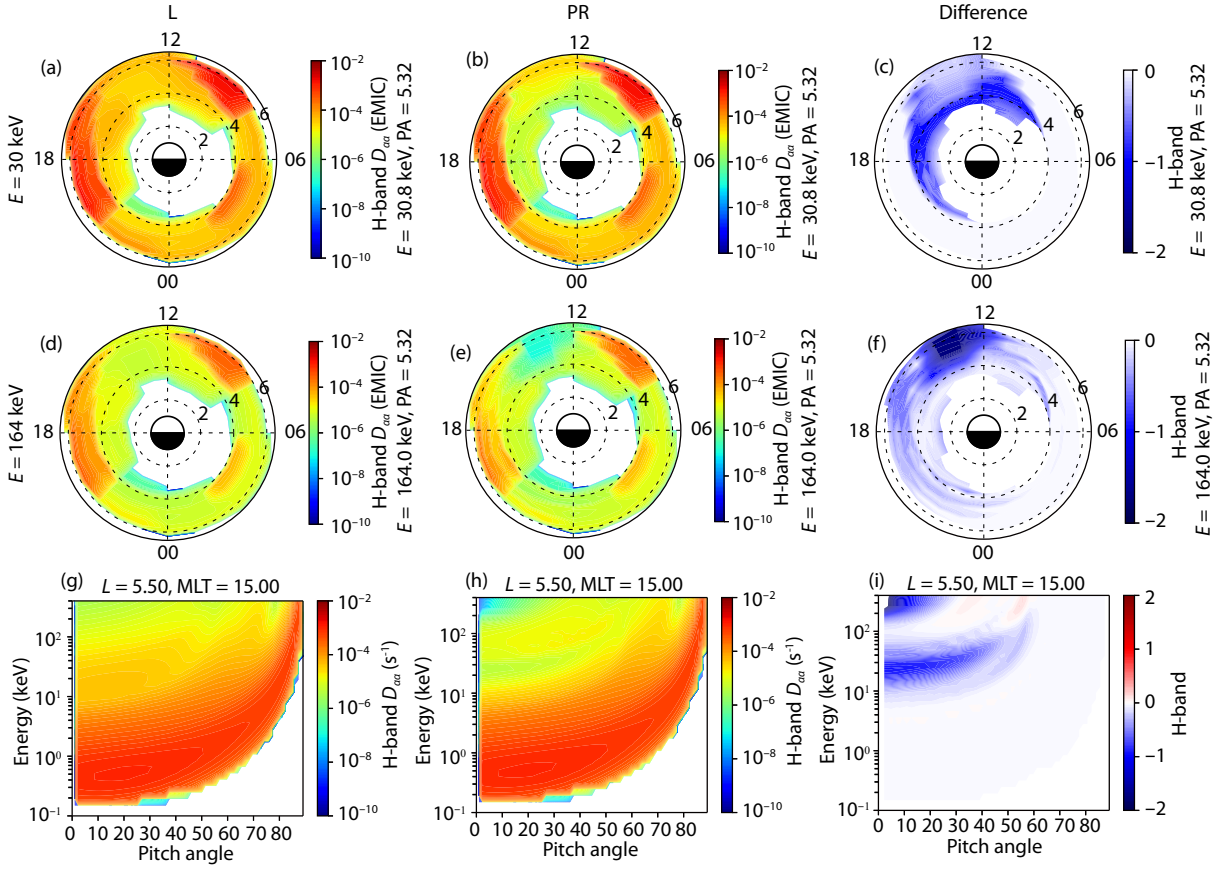

Figure 2. The global distribution of bounce-averaged pitch angle diffusion coefficients $\langle D_{\alpha\alpha}\rangle$ with (a, d) pure left-handed (L) and (b, e) polarization-reversed (PR) H-band electromagnetic ion cyclotron waves and (c, f) the difference in magnitude at pitch angle (PA) $\alpha = 5^{\circ}$ at 10:30 universal time (UT). The corresponding energies are 30 and 164 keV, respectively. The $\langle D_{\alpha\alpha}\rangle$ of (g) pure left-handed (L) and (h) polarization-reversed (PR) H-band waves as functions of energy and pitch angle at $L = 5.5$, magnetic local time (MLT) = 15, and (i) their difference of magnitude.

Figures 5a and 5b show the global precipitation flux for the pure L-mode case and the difference in the precipitating flux between the two cases during the prestorm, main phase, and recovery phase. The ion precipitation mainly occurs outside $L = 4$ in the dusk-to-dawn sector across noon in the prestorm and the recovery phase, and the occurrence is global during the main phase of the storm. Inclusion of the polarization reversal causes a decrease in the global precipitating flux (blue), although a slight increase in the flux (red) is seen during the recovery phase, especially outside the plasmapause in the dawn sector. The magnitude difference between the two cases is about 0.5 or less, which is not a significant change for the total ring current energy content. Although the global distribution of the precipitating flux varies in different periods of the magnetic storm, the overall variation is small. The maximum local variation is within one order of magnitude, which means the precipitation loss of the ring current is not greatly affected. The total ring current pressure in the pure L-mode case and the relative difference between the two cases are shown in Figures 5c and 5d. In Figure 5d, the relative difference is calculated as $D_{pressure} = (P_{PR} - P_{PL})/P_{PL} \times 100\%$, where P_{PL} and P_{PR} are the pressure in the pure L-mode and in the polarization-reversed mode. The ring current pressure can be seen to increase with the development of the storm and can reach approximately 10%, which suggests a negligible impact. It should be noted that these simulations use simple magnetic and electric field models, but the above conclusion that the precipitation loss and ring current intensity are not substantially affected does not change even if we change the electromagnetic field models to be more sophisticated and self-consistent.

4. Conclusions

Previous studies have shown that polarization-reversed EMIC waves can enhance the scattering loss of several mega electron volt radiation belt electrons and reduce the loss rates of ring current protons over a broad energy range from a few kiloelectron volt to >100 keV. The decrease in the proton diffusion coefficient can be as large as one order of magnitude (Cao X et al., 2020; Lou YQ et al., 2021). How such changes in the diffusion loss rates resulting from the inclusion of polarization reversal alter the global ring current dynamics needs further investigation. In this study, we simulated the storm event of March 17, 2013, by using the RAM model and incorporating the EMIC wave-scattering effects on the ring current protons either by using a pure L-mode or by including the polarization-reversed mode. By comparing the results under the two polarization modes, we achieved the following results:

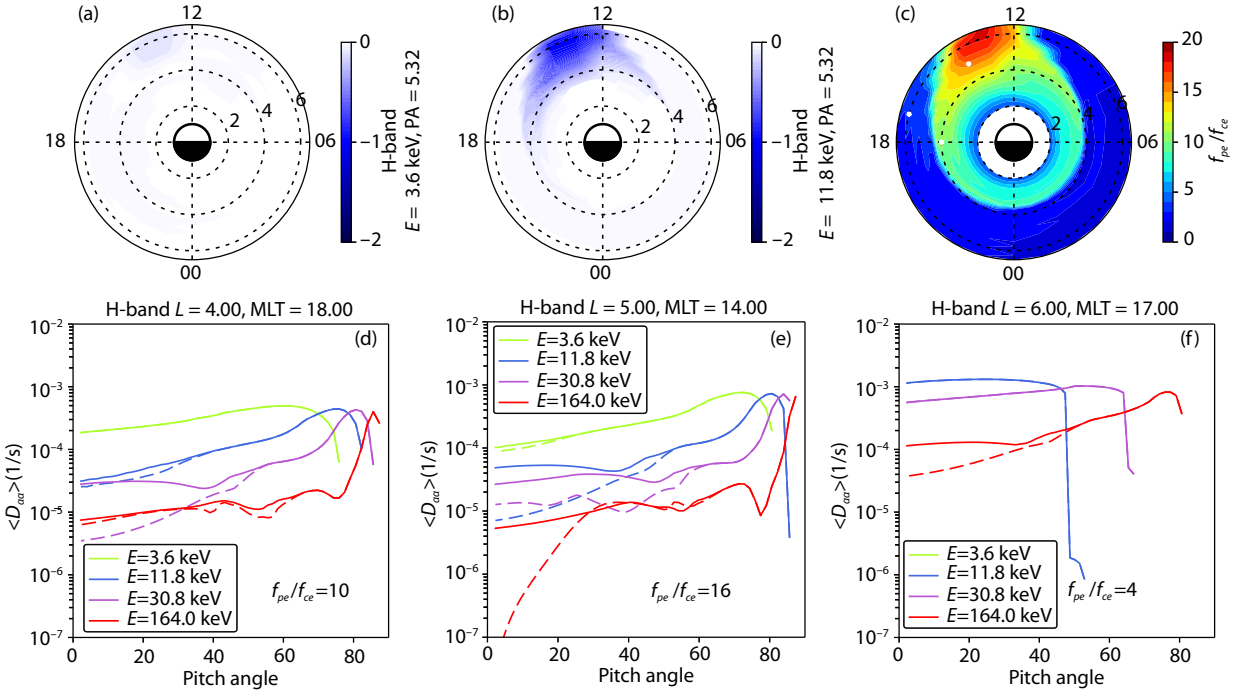

Figure 3. (a, b) The global distribution of the magnitude difference between the pitch angle diffusion coefficients $\langle D_{\alpha\alpha}\rangle$ with pure left-handed polarization and polarization reversal at pitch angle (PA) $\alpha = 5^\circ$, $E = 3.6$, and 11.8 keV at 10:30 UT. (c) The global distribution of f_{pe}/f_{ce}. (d–f) The $\langle D_{\alpha\alpha}\rangle$ as a function of pitch angle with different energies at three selected locations marked by the white dots in (c). The solid lines represent pure left-handed polarization, and the dashed lines represent polarization reversal.

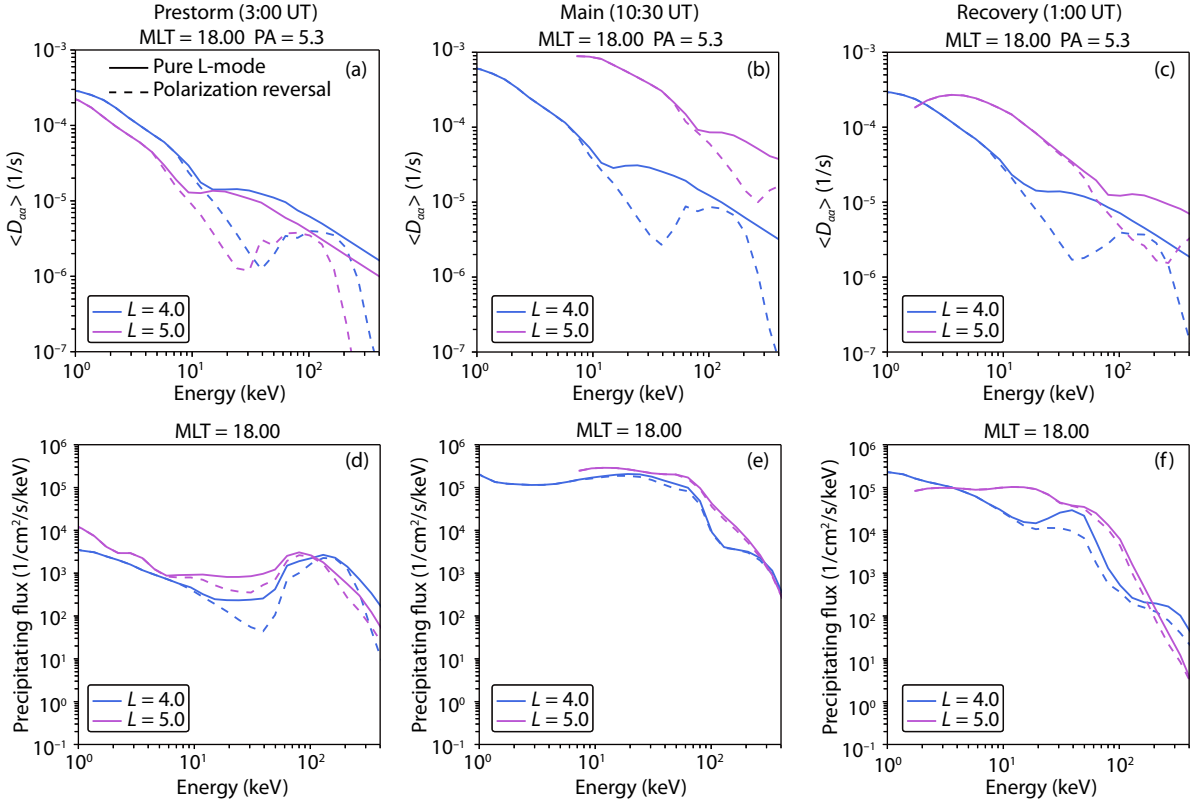

Figure 4. (a–c) Variation in the pitch angle diffusion coefficient $\langle D_{\alpha\alpha}\rangle$ with energy at pitch angle (PA) $\alpha = 5^\circ$, magnetic local time (MLT) = 18 at 3:00 UT, 10:30 universal time (UT), and 1:00 UT (on the next day), respectively. (d–f) Variation in the precipitating flux with energy at MLT = 18 at the three times. The solid lines represent pure left-handed polarization, and the dashed lines represent polarization reversal. The blue and purple lines indicate $L = 4$, 5.

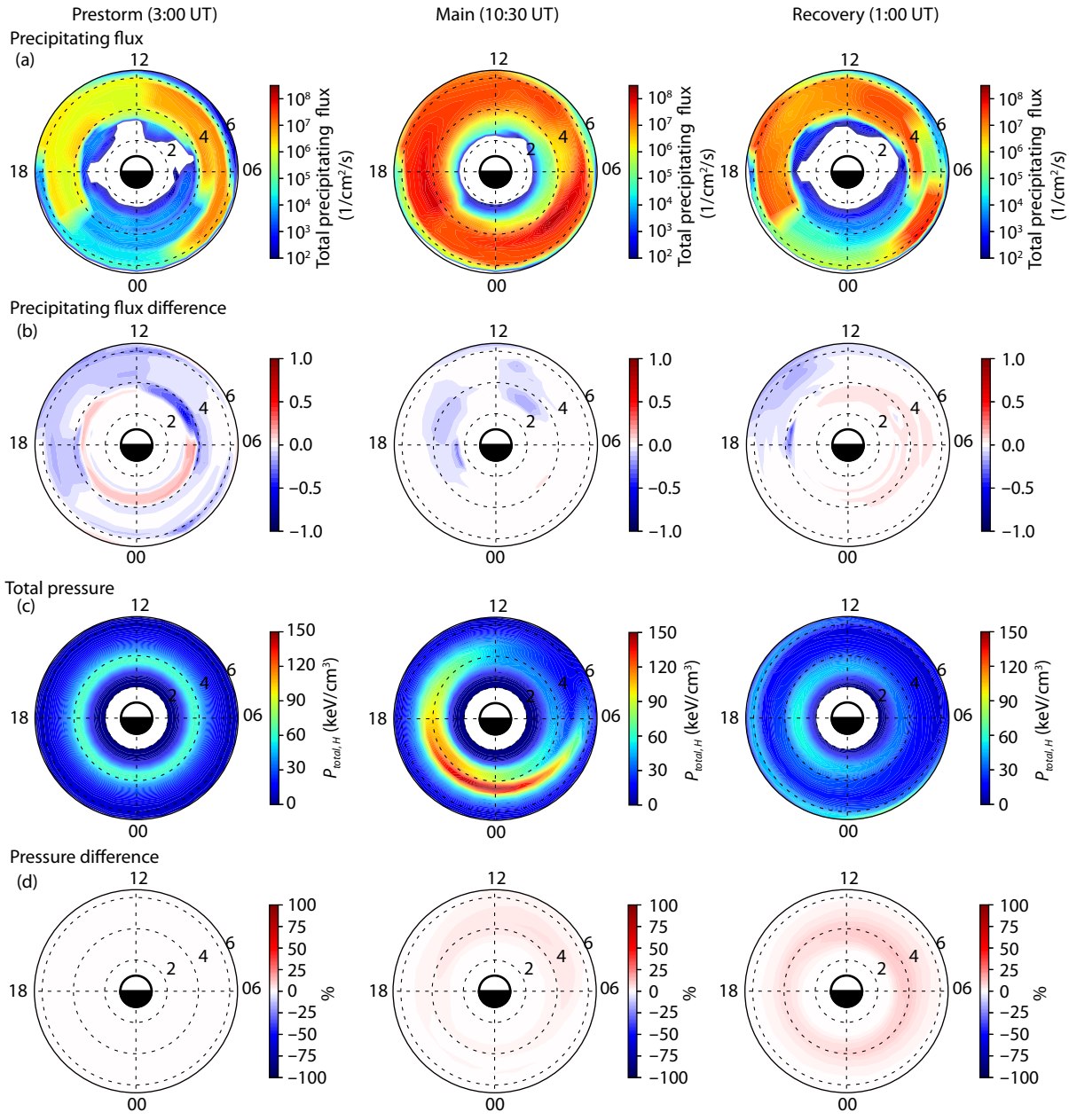

Figure 5. (a) The precipitating flux for the pure left-handed (L)-mode and (b) the magnitude difference of the precipitating flux between the pure L-mode and the polarization-reversed H-band electromagnetic ion cyclotron waves in global distribution at 3:00 universal time (UT), 10:30 UT, and 1:00 UT (on the next day). (c) The total ring current pressure in the pure L-mode and (d) the relative difference in global distribution between the two cases at 3:00 UT, 10:30 UT, and 1:00 UT (on the next day).

(1) The bounce-averaged pitch angle diffusion coefficients $\langle D_{\alpha\alpha}\rangle$ are reduced for a few kiloelectron volt to hundreds of kiloelectron volt protons when the polarization reversal is included, as opposed to that of the pure left-handed polarization, but the affected region is different for different energies. For a few kiloelectron volt to tens of kiloelectron volt protons, $\langle D_{\alpha\alpha}\rangle$ decreases in the noon and afternoon sectors inside the plasmapause, whereas the coefficient for energies >100 keV is mainly reduced in regions with a much smaller plasmasphere density or regions with a much higher density (e.g., the plume).

(2) Although the diffusion coefficients associated with the polarization reversal are generally lower than those of the pure L-mode, by a factor of 5–10 at different energies, the change in the global proton precipitating flux is not substantial, meaning that the scattering loss of the ring current protons is not greatly affected from a global perspective, especially during the main phase of the storm. This is probably because the most significant impact of the polarization reversal occurs at $E > 100$ keV, but the scattering loss attributable to the EMIC waves is most efficient at $E < 10$ keV.

It should be noted that the calculation of the EMIC wave-induced diffusion rates is not yet self-consistent with the ring current dynamics because of the extensive resources required in the calculation. In addition, the precalculated rates are based on simplified or fixed-parameter settings, such as ion compositions,

magnetic configurations, electron number density, and wave spectra. Lou YQ et al. (2021) actually found that varying these parameters can introduce significant differences in the diffusion rates between the pure L-mode and polarization-reversal approaches, in terms of the efficient resonant energy and pitch angle. Such variations can result in changes in the affected energy range from a few kiloelectron volts to hundreds of kiloelectron volts, but the magnitude of the variation between the two wave modes is not greatly affected. Therefore, we believe that the effects of varying the parameters may not change the conclusion.

Acknowledgments

This work was supported by the National Natural Science Foundation of China (Grant Nos. 41974192 and 41821003). Work at Los Alamos was performed under the auspices of the U.S. Department of Energy (Contract No. 89233218CNA000001) and was partially funded by an NSF grant (Grant No. IAA2027951). The authors thank the National Aeronautics and Space Administration (NASA) Goddard Space Flight Center for providing the solar wind and interplanetary magnetic field data, SYM-*H* index, and *AE* index from the OMNIWeb (http://omniweb.gsfc.nasa.gov/). Simulations were performed on TianHe-2 at the National Supercomputer Center in Guangzhou, China. The RAM-SCB model code is available at https://github.com/lanl/RAM-SCB.

References

Albert, J. M. (2003). Evaluation of quasi-linear diffusion coefficients for EMIC waves in a multispecies plasma. *J. Geophys. Res.*: *Space Phys.*, *108*(A6), 1249. https://doi.org/10.1029/2002JA009792

Allen, R. C., Zhang, J. C., Kistler, L. M., Spence, H. E., Lin, R. L., Klecker, B., Dunlop, M. W., André, M., and Jordanova, V. K. (2015). A statistical study of EMIC waves observed by Cluster: 1. Wave properties. *J. Geophys. Res.*: *Space Phys.*, *120*(7), 5574–5592. https://doi.org/10.1002/2015JA021333

Allen, R. C., Zhang, J. C., Kistler, L. M., Spence, H. E., Lin, R. L., Klecker, B., Dunlop, M. W., André, M., and Jordanova, V. K. (2016). A statistical study of EMIC waves observed by Cluster: 2. Associated plasma conditions. *J. Geophys. Res.*: *Space Phys.*, *121*(7), 6458–6479. https://doi.org/10.1002/2016JA022541

Anderson, B. J., Erlandson, R. E., and Zanetti, L. J. (1992). A statistical study of Pc 1-2 magnetic pulsations in the equatorial magnetosphere: 2. Wave properties. *J. Geophys. Res.*: *Space Phys.*, *97*(A3), 3089–3101. https://doi.org/10.1029/91JA02697

Anderson, B. J., Denton, R. E., Ho, G., Hamilton, D. C., Fuselier, S. A., and Strangeway, R. J. (1996). Observational test of local proton cyclotron instability in the Earth's magnetosphere. *J. Geophys. Res.*: *Space Phys.*, *101*(A10), 21527–21543. https://doi.org/10.1029/96JA01251

Blum, L. W., Remya, B., Denton, M. H., and Schiller, Q. (2020). Persistent EMIC wave activity across the nightside inner magnetosphere. *Geophys. Res. Lett.*, *47*(6), e2020GL087009. https://doi.org/10.1029/2020GL087009

Cao, X., Ni, B. B., Liang, J., Xiang, Z., Wang, Q., Shi, R., Gu, X. D., Zhou, C., Zhao, Z. Y., … Liu, J. (2016). Resonant scattering of central plasma sheet protons by multiband EMIC waves and resultant proton loss timescales. *J. Geophys. Res.*: *Space Phys.*, *121*(2), 1219–1232. https://doi.org/10.1002/2015JA021933

Cao, X., Ni, B. B., Summers, D., Shprits, Y. Y., Gu, X. D., Fu, S., Lou, Y. Q., Zhang, Y., Ma, X., … Yi, J. (2019). Sensitivity of EMIC wave-driven scattering loss of ring current protons to wave normal angle distribution. *Geophys. Res. Lett.*, *46*(2), 590–598. https://doi.org/10.1029/2018GL081550

Cao, X., Ni, B. B., Summers, D., Shprits, Y. Y., and Lou, Y. Q. (2020). Effects of polarization reversal on the pitch angle scattering of radiation belt electrons and ring current protons by EMIC waves. *Geophys. Res. Lett.*, *47*(17), e2020GL089718. https://doi.org/10.1029/2020GL089718

Capannolo, L., Li, W., Ma, Q. L., Shen, X. C., Zhang, X. J., Redmon, R. J., Rodriguez, J. V., Engebretson, M. J., Kletzing, C. A., …Raita, T. (2019). Energetic electron precipitation: Multievent analysis of its spatial extent during EMIC wave activity. *J. Geophys. Res.*: *Space Phys.*, *124*(4), 2466–2483. https://doi.org/10.1029/2018JA026291

Cornwall, J. M. (1965). Cyclotron instabilities and electromagnetic emission in the ultra low frequency and very low frequency ranges. *J. Geophys. Res.*, *70*(1), 61–69. https://doi.org/10.1029/JZ070i001p00061

Cornwall, J. M. (1972). Precipitation of auroral and ring current particles by artificial plasma injection. *Rev. Geophys.*, *10*(4), 993–1002. https://doi.org/10.1029/RG010i004p00993

Engebretson, M. J., Posch, J. L., Capman, N. S. S., Campuzano, N. G., Bělik, P., Allen, R. C., Vines, S. K., Anderson, B. J., Tian, S., … Singer, H. J. (2018a). MMS, Van Allen Probes, GOES 13, and ground-based magnetometer observations of EMIC wave events before, during, and after a modest interplanetary shock. *J. Geophys. Res.*: *Space Phys.*, *123*(10), 8331–8357. https://doi.org/10.1029/2018JA025984

Engebretson, M. J., Posch, J. L., Braun, D. J., Li, W., Ma, Q. L., Kellerman, A. C., Huang, C. L., Kanekal, S. G., Kletzing, C. A., … Ermakova, E. (2018b). EMIC wave events during the four GEM QARBM challenge intervals. *J. Geophys. Res.*: *Space Phys.*, *123*(8), 6394–6423. https://doi.org/10.1029/2018JA025505

Glauert, S. A., and Horne, R. B. (2005). Calculation of pitch angle and energy diffusion coefficients with the PADIE code. *J. Geophys. Res.*: *Space Phys.*, *110*(A4), A04206. https://doi.org/10.1029/2004JA010851

He, F. M., Cao, X., Ni, B. B., Xiang, Z., Zhou, C., Gu, X. D., Zhao, Z. Y., Shi, R., and Wang, Q. (2016). Combined scattering loss of radiation belt relativistic electrons by simultaneous three-band EMIC waves: A case study. *J. Geophys. Res.*: *Space Phys.*, *121*(5), 4446–4451. https://doi.org/10.1002/2016JA022483

Hendry, A. T., Rodger, C. J., Clilverd, M. A., Engebretson, M. J., Mann, I. R., Lessard, M. R., Raita, T., and Milling, D. K. (2016). Confirmation of EMIC wave-driven relativistic electron precipitation. *J. Geophys. Res.*: *Space Phys.*, *121*(6), 5366–5383. https://doi.org/10.1002/2015JA022224

Horne, R. B., and Thorne, R. M. (1994). Convective instabilities of electromagnetic ion cyclotron waves in the outer magnetosphere. *J. Geophys. Res.*: *Space Phys.*, *99*(A9), 17259–17273. https://doi.org/10.1029/94JA01259

Hu, Y. G., Denton, R. E., and Johnson, J. R. (2010). Two-dimensional hybrid code simulation of electromagnetic ion cyclotron waves of multi-ion plasmas in a dipole magnetic field. *J. Geophys. Res.*: *Space Phys.*, *115*(A9), A09218. https://doi.org/10.1029/2009JA015158

Jordanova, V. K., Kozyra, J. U., and Nagy, A. F. (1996). Effects of heavy ions on the quasi-linear diffusion coefficients from resonant interactions with electromagnetic ion cyclotron waves. *J. Geophys. Res.*: *Space Phys.*, *101*(A9), 19771–19778. https://doi.org/10.1029/96JA01641

Jordanova, V. K., Farrugia, C. J., Thorne, R. M., Khazanov, G. V., Reeves, G. D., and Thomsen, M. F. (2001). Modeling ring current proton precipitation by electromagnetic ion cyclotron waves during the May 14–16, 1997, storm. *J. Geophys. Res.*: *Space Phys.*, *106*(A1), 7–22. https://doi.org/10.1029/2000JA002008

Jordanova, V. K., Miyoshi, Y. S., Zaharia, S., Thomsen, M. F., Reeves, G. D., Evans, D. S., Mouikis, C. G., and Fennell, J. F. (2006). Kinetic simulations of ring current evolution during the Geospace Environment Modeling challenge events. *J. Geophys. Res.*: *Space Phys.*, *111*(A11), A11S10. https://doi.org/10.1029/2006JA011644

Jordanova, V. K., Albert, J., and Miyoshi, Y. (2008). Relativistic electron precipitation by EMIC waves from self-consistent global simulations. *J. Geophys. Res.*: *Space Phys.*, *113*(A3), A00A10. https://doi.org/10.1029/2008JA013239

Jordanova, V. K., Zaharia, S., and Welling, D. T. (2010). Comparative study of ring current development using empirical, dipolar, and self-consistent magnetic field simulations. *J. Geophys. Res.*: *Space Phys.*, *115*(A12), A00J11. https://doi.org/10.1029/2010JA015671

Jun, C. W., Yue, C., Bortnik, J., Lyons, L. R., Nishimura, Y. T., Kletzing, C. A., Wygant, J., and Spence, H. (2019). A statistical study of EMIC waves associated with and without energetic particle injection from the magnetotail. *J. Geophys. Res.*: *Space Phys.*, *124*(1), 433–450. https://doi.org/

10.1029/2018JA025886

Kennel, C. F., and Petschek, H. E. (1966). Limit on stably trapped particle fluxes. *J. Geophys. Res.*, *71*(1), 1–28. https://doi.org/10.1029/JZ071i001p00001

Kersten, T., Horne, R. B., Glauert, S. A., Meredith, N. P., Fraser, B. J., and Grew, R. S. (2014). Electron losses from the radiation belts caused by EMIC waves. *J. Geophys. Res.*: *Space Phys.*, *119*(11), 8820–8837. https://doi.org/10.1002/2014JA020366

Kim, H., Shiokawa, K., Park, J., Miyoshi, Y., Miyashita, Y., Stolle, C., Kim, K. H., Matzka, J., Buchert, S., … Hwang, J. (2020). Ionospheric plasma density oscillation related to EMIC Pc1 waves. *Geophys. Res. Lett.*, *47*(15), e2020GL089000. https://doi.org/10.1029/2020GL089000

Kitamura, N., Kitahara, M., Shoji, M., Miyoshi, Y., Hasegawa, H., Nakamura, S., Katoh, Y., Saito, Y., Yokota, S., … Burch, J. L. (2018). Direct measurements of two-way wave-particle energy transfer in a collisionless space plasma. *Science*, *361*(6406), 1000–1003. https://doi.org/10.1126/science.aap8730

Kozyra, J. U., Cravens, T. E., Nagy, A. F., Fontheim, E. G., and Ong, R. S. B. (1984). Effects of energetic heavy ions on electromagnetic ion cyclotron wave generation in the plasmapause region. *J. Geophys. Res.*: *Space Phys.*, *89*(A4), 2217–2233. https://doi.org/10.1029/JA089iA04p02217

Kwon, J. W., Kim, K. H., Jin, H., Kwon, H. J., Jee, G., Shiokawa, K., and Connors, M. (2020). Statistical study of EMIC Pc1-Pc2 waves observed at subauroral latitudes. *J. Atmos. Sol.-Terr. Phys.*, *205*, 105292. https://doi.org/10.1016/j.jastp.2020.105292

Li, L. Y., Yu, J., Cao, J. B., and Yuan, Z. G. (2016). Compression-amplified EMIC waves and their effects on relativistic electrons. *Phys. Plasmas*, *23*(6), 062116. https://doi.org/10.1063/1.4953899

Lou, Y. Q., Cao, X., Ni, B. B., Wu, M. Y., and Zhang, T. L. (2021). Parametric dependence of polarization reversal effects on the particle pitch angle scattering by EMIC waves. *J. Geophys. Res.*: *Space Phys.*, *126*(12), e2021JA029966. https://doi.org/10.1029/2021JA029966

Lyons, L. R., and Thorne, R. M. (1972). Parasitic pitch angle diffusion of radiation belt particles by ion cyclotron waves. *J. Geophys. Res.*, *77*(28), 5608–5616. https://doi.org/10.1029/JA077i028p05608

Ma, Q. L., Li, W., Yue, C., Thorne, R. M., Bortnik, J., Kletzing, C. A., Kurth, W. S., Hospodarsky, G. B., Reeves, G. D., and Spence, H. E. (2019). Ion heating by electromagnetic ion cyclotron waves and magnetosonic waves in the Earth's inner magnetosphere. *Geophys. Res. Lett.*, *46*(12), 6258–6267. https://doi.org/10.1029/2019GL083513

Ma, X., Xiang, Z., Ni, B. B., Fu, S., Cao, X., Hua, M., Guo, D. Y., Guo, Y. J., Gu, X. D., Liu, Z. Y. and Zhu, Q. (2020). On the loss mechanisms of radiation belt electron dropouts during the 12 September 2014 geomagnetic storm. *Earth Planet. Phys.*, *4*(6), 598–610. https://doi.org/10.26464/epp2020060

Mauk, B. H., and McPherron, R. L. (1980). An experimental test of the electromagnetic ion cyclotron instability within the Earth's magnetosphere. *Phys. Fluids*, *23*(10), 2111–2127. https://doi.org/10.1063/1.862873

Min, K., Lee, J., Keika, K., and Li, W. (2012). Global distribution of EMIC waves derived from THEMIS observations. *J. Geophys. Res.*: *Space Phys.*, *117*(A5), A05219. https://doi.org/10.1029/2012JA017515

Ni, B. B., Thorne, R. M., Shprits, Y. Y., and Bortnik, J. (2008). Resonant scattering of plasma sheet electrons by whistler-mode chorus: Contribution to diffuse auroral precipitation. *Geophys. Res. Lett.*, *35*(11), L11106. https://doi.org/10.1029/2008GL034032

Ni, B. B., Thorne, R. M., Meredith, N. P., Horne, R. B., and Shprits, Y. Y. (2011). Resonant scattering of plasma sheet electrons leading to diffuse auroral precipitation: 2. Evaluation for whistler mode chorus waves. *J. Geophys. Res.*: *Space Phys.*, *116*(A4), A04219. https://doi.org/10.1029/2010JA016233

Ni, B. B., Cao, X., Zou, Z. Y., Zhou C., Gu, X. D., Bortnik, J., Zhang, J. C., Fu, S., Zhao, Z. Y., … Xie, L. (2015). Resonant scattering of outer zone relativistic electrons by multiband EMIC waves and resultant electron loss time scales. *J. Geophys. Res.*: *Space Phys.*, *120*(9), 7357–7373. https://doi.org/10.1002/2015JA021466

Ni, B. B., Cao, X., Shprits, Y. Y., Summers, D., Gu, X. D., Fu, S., and Lou, Y. Q. (2018). Hot plasma effects on the cyclotron-resonant pitch-angle scattering rates of radiation belt electrons due to EMIC waves. *Geophys. Res. Lett.*, *45*(1), 21–30. https://doi.org/10.1002/2017GL076028

Perraut, S., Gendrin, R., Roux, A., and de Villedary, C. (1984). Ion cyclotron waves: Direct comparison between ground-based measurements and observations in the source region. *J. Geophys. Res.*: *Space Phys.*, *89*(A1), 195–202. https://doi.org/10.1029/JA089iA01p00195

Rauch, J. L., and Roux, A. (1982). Ray tracing of ULF waves in a multicomponent magnetospheric plasma: Consequences for the generation mechanism of ion cyclotron waves. *J. Geophys. Res.*: *Space Phys.*, *87*(A10), 8191–8198. https://doi.org/10.1029/JA087iA10p08191

Saikin, A. A., Zhang, J. C., Allen, R. C., Smith, C. W., Kistler, L. M., Spence, H. E., Torbert, R. B., Kletzing, C. A., and Jordanova, V. K. (2015). The occurrence and wave properties of H^+-, He^+-, and O^+-band EMIC waves observed by the Van Allen Probes. *J. Geophys. Res.*: *Space Phys.*, *120*(9), 7477–7492. https://doi.org/10.1002/2015JA021358

Saikin, A. A. (2018). The spatial distributions, wave properties, and generation mechanisms of inner magnetosphere EMIC waves [Ph. D. thesis]. Durham: University of New Hampshire.

Sheeley, B. W., Moldwin, M. B., Rassoul, H. K., and Anderson, R. R. (2001). An empirical plasmasphere and trough density model: CRRES observations. *J. Geophys. Res.*: *Space Phys.*, *106*(A11), 25631–25641. https://doi.org/10.1029/2000JA000286

Shprits, Y. Y., and Ni, B. B. (2009). Dependence of the quasi-linear scattering rates on the wave normal distribution of chorus waves. *J. Geophys. Res.*: *Space Phys.*, *114*(A11), A11205. https://doi.org/10.1029/2009JA014223

Shreedevi, P. R., Yu, Y. Q., Ni, B. B., Saikin, A., and Jordanova, V. K. (2021). Simulating the ion precipitation from the inner magnetosphere by H-band and He-band electro magnetic ion cyclotron waves. *J. Geophys. Res.*: *Space Phys.*, *126*(3), e2020JA028553. https://doi.org/10.1029/2020JA028553

Stern, D. P. (1975). The motion of a proton in the equatorial magnetosphere. *J. Geophys. Res.*, *80*(4), 595–599. https://doi.org/10.1029/JA080i004p00595

Su, Z. P., Zhu, H., Xiao, F. L., Zheng, H. N., Shen, C., Wang, Y. M., and Wang, S. (2013). Latitudinal dependence of nonlinear interaction between electromagnetic ion cyclotron wave and radiation belt relativistic electrons. *J. Geophys. Res.*: *Space Phys.*, *118*(6), 3188–3202. https://doi.org/10.1002/jgra.50289

Summers, D., and Thorne, R. M. (2003). Relativistic electron pitch-angle scattering by electromagnetic ion cyclotron waves during geomagnetic storms. *J. Geophys. Res.*: *Space Phys.*, *108*(A4), 1143. https://doi.org/10.1029/2002JA009489

Summers, D., Ni, B. B., and Meredith, N. P. (2007). Timescales for radiation belt electron acceleration and loss due to resonant wave-particle interactions: 1. Theory. *J. Geophys. Res.*: *Space Phys.*, *112*(A4), A04206. https://doi.org/10.1029/2006JA011801

Thorne, R. M., and Horne, R. B. (1997). Modulation of electromagnetic ion cyclotron instability due to interaction with ring current O^+ during magnetic storms. *J. Geophys. Res.*: *Space Phys.*, *102*(A7), 14155–14163. https://doi.org/10.1029/96JA04019

Usanova, M. E., Drozdov, A., Orlova, K., Mann, I. R., Shprits, Y., Robertson, M. T., Turner, D. L., Milling, D. K., Kale, A., … Wygant, J. (2014). Effect of EMIC waves on relativistic and ultrarelativistic electron populations: Ground-based and Van Allen Probes observations. *Geophys. Res. Lett.*, *41*(5), 1375–1381. https://doi.org/10.1002/2013GL059024

Volland, H. (1973). A semiempirical model of large-scale magnetospheric electric fields. *J. Geophys. Res.*, *78*(1), 171–180. https://doi.org/10.1029/JA078i001p00171

Wang, Q., Cao, X., Gu, X. D., Ni, B. B., Zhou, C., Shi, R., and Zhao, Z. Y. (2016). A parametric study of the linear growth of magnetospheric EMIC waves in a hot plasma. *Phys. Plasmas*, *23*(6), 062903. https://doi.org/10.1063/1.4953565

Wang, X. Y., Huang, S. Y., Allen, R. C., Fu, H. S., Deng, X. H., Zhou, M., Burch, J. L., and Torbert, R. B. (2017). The occurrence and wave properties of EMIC waves observed by the Magnetospheric Multiscale (MMS) mission. *J. Geophys. Res.*: *Space Phys.*, *122*(8), 8228–8240. https://doi.org/10.1002/2017JA024237

Xiao, F. L., Chen, L. X., He, Y. H., Su, Z. P., and Zheng, H. N. (2011). Modeling for precipitation loss of ring current protons by electromagnetic ion cyclotron waves. *J. Atmos. Sol.-Terr. Phys.*, *73*(1), 106–111. https://doi.org/10.1016/j.jastp.2010.01.007

Xiao, F. L., Yang, C., Zhou, Q. H., He, Z. G., He, Y. H., Zhou, X. P., and Tang, L. J. (2012). Nonstorm time scattering of ring current protons by electromagnetic ion cyclotron waves. *J. Geophys. Res.*: *Space Phys.*, *117*(A8), A08204. https://doi.org/10.1029/2012JA017922

Xue, Z. X., Yuan, Z. G., Yu, X. D., Huang, S. Y. and Qiao, Z. (2021). Formation of the mass density peak at the magnetospheric equator triggered by EMIC waves. *Earth Planet. Phys.*, *5*(1), 32–41. https://doi.org/10.26464/epp2021008

Young, D. T., Perraut, S., Roux, A., de Villedary, C., Gendrin, R., Korth, A., Kremser, G., and Jones, D. (1981). Wave–particle interactions near Ω_{He^+} observed on GEOS 1 and 2. 1. Propagation of ion cyclotron waves in He^+-rich plasma. *J. Geophys. Res.*: *Space Phys.*, *86*(A8), 6755–6772. https://doi.org/10.1029/JA086iA08p06755

Yuan, Z. G., Deng, X. H., Lin, X., Pang, Y., Zhou, M., Décréau, P. M. E., Trotignon, J. G., Lucek, E., Frey, H. U., and Wang, J. F. (2010). Link between EMIC waves in a plasmaspheric plume and a detached sub-auroral proton arc with observations of Cluster and IMAGE satellites. *Geophys. Res. Lett.*, *37*(7), L07108. https://doi.org/10.1029/2010GL042711

Yue, C., Jun, C. W., Bortnik, J., An, X., Ma, Q. L., Reeves, G. D., Spence, H. E., Gerrard, A. J., Gkioulidou, M., ... Kletzing, C. A. (2019). The relationship between EMIC wave properties and proton distributions based on Van Allen probes observations. *Geophys. Res. Lett.*, *46*(8), 4070–4078. https://doi.org/10.1029/2019GL082633

Zaharia, S., Jordanova, V. K., Thomsen, M. F., and Reeves, G. D. (2006). Self-consistent modeling of magnetic fields and plasmas in the inner magnetosphere: Application to a geomagnetic storm. *J. Geophys. Res.*: *Space Phys.*, *111*(A11), A11S14. https://doi.org/10.1029/2006JA011619

Zaharia, S., Jordanova, V. K., Welling, D., and Tóth, G. (2010). Self-consistent inner magnetosphere simulation driven by a global MHD model. *J. Geophys. Res.*: *Space Phys.*, *115*(A12), A12228. https://doi.org/10.1029/2010JA015915

Zhang, J. C., Kistler, L. M., Mouikis, C. G., Dunlop, M. W., Klecker, B., and Sauvaud, J. A. (2010). A case study of EMIC wave-associated He^+ energization in the outer magnetosphere: Cluster and Double Star 1 observations. *J. Geophys. Res.*: *Space Phys.*, *115*(A6), A06212. https://doi.org/10.1029/2009JA014784

Zhu, M. H., Yu, Y. Q., Tian, X. B., Shreedevi, P. R., and Jordanova, V. K. (2021a). On the ion precipitation due to field line curvature (FLC) and EMIC wave scattering and their subsequent impact on ionospheric electrodynamics. *J. Geophys. Res.*: *Space Phys.*, *126*(3), e2020JA028812. https://doi.org/10.1029/2020JA028812

Zhu, M. H., Yu, Y. Q., and Jordanova, V. K. (2021b). Simulating the effects of warm O^+ ions on the growth of electromagnetic ion cyclotron (EMIC) waves. *J. Atmos. Sol.-Terr. Phys.*, *224*, 105737. https://doi.org/10.1016/j.jastp.2021.105737